The TRGB Distance to the Second Galaxy "Missing Dark Matter": Evidence for Two Groups of Galaxies at 13.5 and 19 Mpc in the Line of Sight of NGC 1052

Matteo Monelli[1,2] and Ignacio Trujillo[1,2]
[1] Instituto de Astrofísica de Canarias (IAC), La Laguna, E-38205, Spain; monelli@iac.es, trujillo@iac.es
[2] Departamento de Astrofísica, Universidad de La Laguna (ULL), E-38200, La Laguna, Spain
Received 2019 March 20; revised 2019 July 1; accepted 2019 July 6; published 2019 July 19

Abstract

A second galaxy "missing dark matter" (NGC 1052-DF4) has been reported recently. Here we show, using the location of the tip of the red giant branch (TRGB), that the distance to this galaxy is 14.2 ± 0.7 Mpc. This locates the galaxy 6 Mpc closer than previously determined. We also analyze the distances to the brightest galaxies in the field of view of NGC 1052. We find that this field is populated by two groups of galaxies in projection: one dominated by NGC 1052 and NGC 1047 at ~19 Mpc, and another group containing NGC 1042 and NGC 1035 (as well as [KKS2000]04 and NGC 1052-DF4) at ~13.5 Mpc. At a distance of 13.5 Mpc the globular clusters of NGC 1052-DF4 have the same properties as globular clusters in the Milky Way and other dwarf galaxies.

Key words: galaxies: evolution – galaxies: formation – galaxies: kinematics and dynamics – galaxies: structure

1. Introduction

The determination of the physical properties of the astronomical objects relies on our ability to have an accurate determination of their distances. However, measuring reliable distances to most of the astronomical sources remains one of the most difficult enterprises in our science. Recently, van Dokkum et al. (2018) and van Dokkum et al. (2019a) reported the presence of two extraordinary low surface brightness galaxies ([KKS2000]04 and NGC 1052-DF4) in the field of view (FOV) of the bright galaxy NGC 1052. These two galaxies are proposed to have a dark matter content compatible with zero. Such a claim is based on the assumption that both galaxies are at a distance of 20 Mpc.

The distance to both dwarf galaxies was measured using the surface brightness fluctuation (SBF) technique. In particular, van Dokkum et al. (2019a) used the calibration provided by Blakeslee et al. (2010) to derive a distance of ~20 Mpc. Unfortunately, the reliability of using a calibration that is established for red and more-massive galaxies to determine the distance to bluer and less-massive galaxies is not at all obvious. In fact, Blakeslee & Cantiello (2018) warned about the use of such a calibration in a range where it has not been explored: "the SBF method is not well-tested at these colors and low stellar densities...". This is a warning that has been vindicated by recent analysis of the SBF methodology exploring low-mass galaxies (see e.g., Cantiello et al. 2018; Carlsten et al. 2019) that directly shows how the extrapolation of Blakeslee et al. (2010) is inaccurate[3] for measuring the distance to these types of galaxies. Fortunately, there are alternative ways to measure the distance to these diffuse systems.

When galaxies are nearby enough so their stellar populations can be resolved into stars, one of the most precise determinations of their distances can be obtained by the location of the tip of the red giant branch (TRGB) in the color–magnitude diagram (CMD) of their stars. In a recent paper (Trujillo et al. 2019), we showed that the location of the TRGB of the CMD of the galaxy [KKS2000]04 (popularized as NGC 1052-DF2)

gives a distance of 13.4 ± 1.1 Mpc.[4] This result was shown to be robust against crowding effects as demonstrated by the fact that the distance to the object was independent to the use of stars in the innermost central region or in the periphery of the object. In this Letter, we analyze the CMD of the other dwarf "lacking dark matter" galaxy: NGC 1052-DF4. We will show that the location of the TRGB of this galaxy puts this object at a distance of 14.2 ± 0.7 Mpc. Finally, we also make an analysis of the distances to the brightest galaxies in the FOV of NGC 1052. We find tantalizing evidence that there are two groups of objects located in the same FOV: one dominated by NGC 1052 at ~19 Mpc, and another one centered on NGC 1042 at ~13.5 Mpc.

2. Data

Hubble Space Telescope (*HST*) imaging of the NGC 1052-DF4 galaxy explored in this work was taken as part of the program GO-14644 (PI: van Dokkum) and consists of two Advanced Camera for Survey (ACS) orbits for each object: one in *F606W* (V_{606}; 2180 s) and one in *F814W* (I_{814}; 2320 s). A first analysis of this data was conducted by Cohen et al. (2018). Data were retrieved from the MAST archive webpage.[5] Each orbit is split into four different images whose individual exposures are of 545 s (*F606W*) and 580 s (*F814W*). The pixel size is 0.″05.

The ACS exposures we used were the ones produced by the standard STScI pipeline: i.e., bias- and dark-current-subtracted, flat-fielded, and with the CTE correction applied. This produces the calibrated "flc" images. To create the CMDs of all the diffuse galaxies we follow the prescriptions given by Monelli et al. (2010). The photometry was made on the individual *flc* images using the DAOPHOT/ALLFRAME set of programs (Stetson 1987, 1994). We extensively masked the background galaxies in our images to remove potential contamination in our catalog by artificial deblending of these sources. Our code performs a simultaneous data reduction of the images of a

---

[3] The extrapolation of the relation provided by Blakeslee et al. (2010) is offset by around 0.55 mag for these bluer and low-mass galaxies. This corresponds to an artificial increase in the distance of ~4.5 Mpc.

[4] Together with another four independent distance indicators, the final distance was established on 13.0 ± 0.4 Mpc.
[5] https://mast.stsci.edu/portal/Mashup/Clients/Mast/Portal.html

given target, assuming individual point spread functions once an input list of stellar objects is provided. The final list of point sources was generated on the stacked median image obtained by registering and co-adding the eight individual available frames (four per filter) of each galaxy. The source detection algorithm was iterated twice. The photometry of the stars is given in the Vega system, adopting the zero-points appropriate for the observations date ($zp_{F606W} = 26.404$, $zp_{F814W} = 25.516$).[6] The photometric catalog was finally cleaned using quality cuts. We used the *sharpness* parameter provided by DAOPHOT, rejecting sources with $|sha| > 0.1$. The use of the *sharpness* parameter for effectively cleaning the sample of false detections (i.e., galaxies, unrecognized doubles, bad pixels, or cosmic rays) has been routinely adopted in the literature (see e.g., Aloisi et al. 2007; Turri et al. 2017).

3. The TRGB Distance to NGC 1052-DF4

An accurate estimate of the distance to the galaxies can be obtained using the TRGB when the stellar populations are resolved (Lee et al. 1993). The TRGB marks the end of the red giant branch (RGB) phase, producing a well-defined discontinuity in the luminosity function (LF) of the stars, which can be easily identified from photometric data. This method has two strong advantages: first, the TRGB is an intrinsically bright feature ($M_I \sim -4$) and, second, the luminosity of the TRGB in the *I/F814W* filters has a very mild dependence on the age and the metallicity (Salaris & Cassisi 1997). For such reasons, the method can be reliably used beyond 10 Mpc. We took the calibration by Rizzi et al. (2007)

$$M_{F814W}^{\mathrm{ACS}} = -4.06 + 0.20 \times [(F606W - F814W) - 1.23]$$

$$(1)$$

which accounts for the mild dependency on the metallicity by taking into account a color term. We applied a color correction to the *F814W* photometry as suggested by McQuinn et al. (2017). This results in a steeper RGB and therefore a better defined TRGB.

The resulting modified and de-reddened CMDs as a function of radius are shown in the left panels of Figure 1. The location of the areas used to explore the CMDs are displayed in Figure 2. Figure 1 shows, from top to bottom, the CMD of sources within $1 R_e$ ($R_e = 16''.5$; Cohen et al. 2018, panel a)), between 1 and $2 R_e$ (panel c)), and within $2 R_e$ (panel e)). The central position of the galaxy was centered at coordinates (R. A. = 02:39:15.1 ; decl. = −08:06:58.6), which corresponds to the pixel position (2868.7, 299.5) of chip 2 of the adopted reference image. The horizontal colored lines mark the position of the TRGB, identified from the LF displayed as a black histogram in the corresponding right panels. The three LFs present a sudden jump at magnitude $F814W_{0,Vega} \approx 26.7$ mag. The statistical significance of this feature (assuming a Poissonian distribution) is 3.2σ (99.86%), 2.2σ (97.2%), and 4.0σ (99.99%) (in panel a), c), and e), respectively). The LF function was convolved with a Sobel kernel (Sakai et al. 1996, 1997) K = [−2, −1, 0, 1, 2]. The position of the apparent magnitude of the TRGB (labeled in the right panels) was derived identifying the peak corresponding to the largest jump in the LF.

The distance modulus was derived with the Rizzi et al. (2007) zero-points, obtaining $(m - M)_0 = 30.76 \pm 0.10$ mag, corresponding to a distance $D = 14.2 \pm 0.7$ Mpc.[7] The final error budget includes the uncertainty of the calibration relation by Rizzi et al. (2007) and the error on the determination of the TRGB position. We also checked how the location of the TRGB would change if, instead of using $|sha| > 0.1$, we used the less-conservative $|sha| > 0.5$. In that case, the location of the TRGB would be brighter by 0.1 mag, making the galaxy closer by 0.7 Mpc (i.e., $D = 13.5 \pm 0.7$ Mpc).

The excellent agreement between the distance determination in the innermost region ($R < R_e$, panel a)) and in a more external annulus ($1 R_e < R < 2 R_e$, panel c)) strongly suggests that the contamination by blends (if any) is marginally affecting our distance estimation. Panel g) of Figure 1 presents the CMD of a control field with an area of 50×50 arcsec^2 located at the coordinates (R.A., decl.) = (02:39:19.2; −08:08:46.7). These coordinates correspond to the pixel position (500, 1500) of chip 2 of the adopted reference image. The center of the control field is about $7.5 R_e$ away from the center of NGC 1052-DF4. The area of the control field (2500 arcsec^2) is chosen to represent an area similar to the one used for exploring the CMD of the galaxy (855 arcsec^2 within $1 R_e$ and 2565 arcsec^2 between 1 and $2 R_e$). The negligible, if any, presence of stars belonging to NGC 1052-DF4 in the location of the control field results in a completely different distribution of sources in its CMD, as well as in the LF peaking at significantly fainter magnitude (panel h), red line).

To further support the fact that the detection of the TRGB is not being significantly affected by noise peaks or possible blends, we have conducted the following diagnostic. We have explored the number of detected stars above and below the TRGB as a function of the radial distance. This is done in Figure 3. As we are using only chip 2 in our analysis, in order to fill the distribution of stars below $-0.9 R_e$ we have mirrored the stars above $+0.9 R_e$. We have divided the detected stars in two groups: asymptotic giant branch stars (AGBs; stars that are brighter than the TRGB) and RGBs (stars that are fainter than the TRGB). Both groups expand 0.5 mag above and below the magnitude of the TRGB. The upper panels of Figure 3 show the spatial location of the AGBs and RGBs around the central position of the galaxy. The lower panels of such figure show the number density of the detected stars as a function of radius. The figure clearly indicates that both AGBs and RGBs tend to cluster around the central part of the galaxy. More importantly, the number density of the stars declines following exactly the same trend as the surface brightness distribution of the object. In Figure 3 we draw both the number density of stars as observed directly (open symbols) and corrected by the incompleteness of the data (filled symbols). Incompleteness simulations were done by injecting a large number of artificial stars (200,000) of different magnitudes across the image. For comparison, we overplotted the surface brightness distribution obtained on the *F814W* using the IRAF ELLIPSE routine (green dotted points) and the Sérsic model fitting solution to the surface brightness distribution obtained by Cohen et al. (2018; red line). As can be seen, the agreement is excellent.
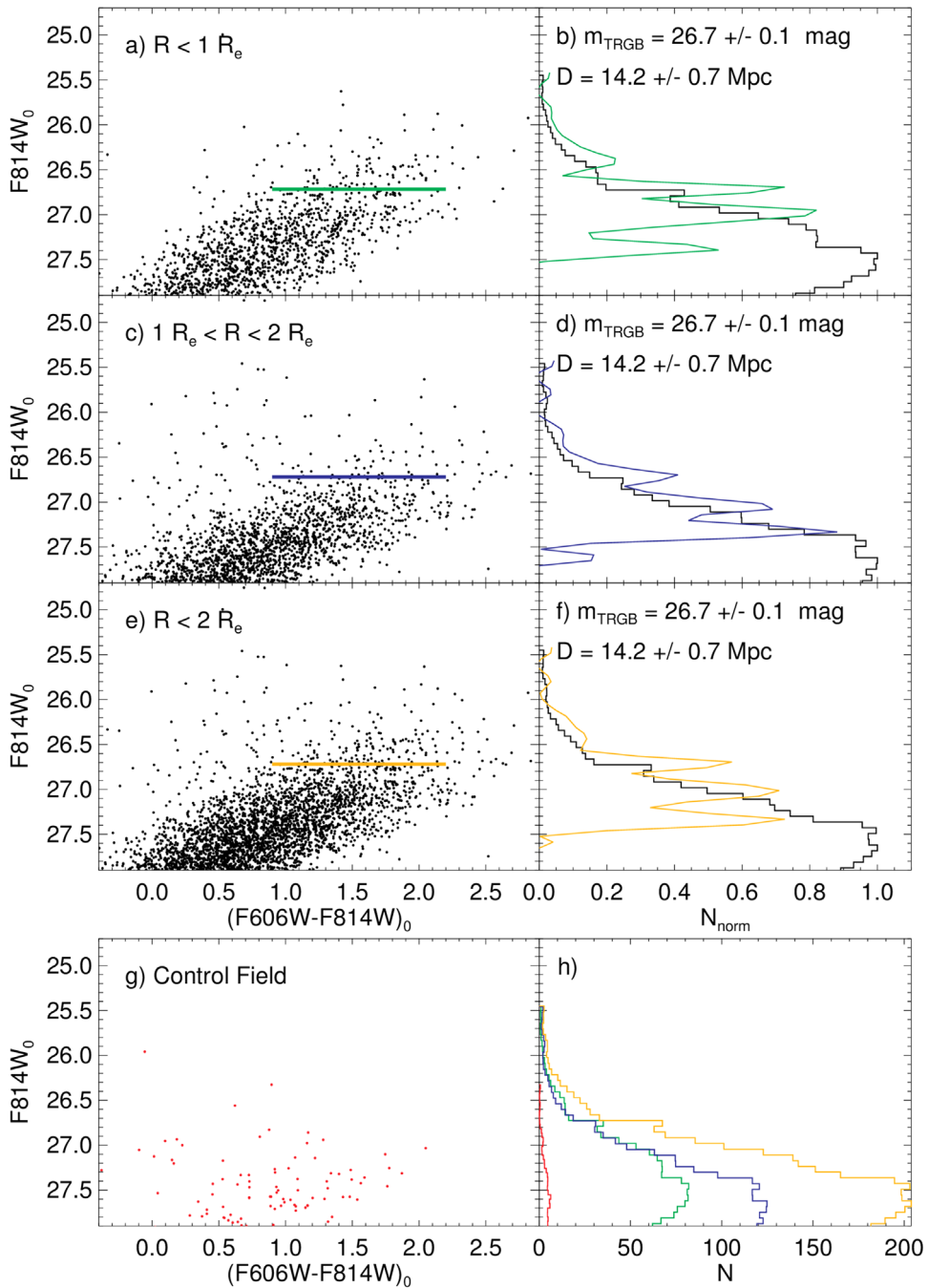
Figure 1. Left panels a), c), and e): de-reddened CMD of NGC 1052-DF4 stars as a function of radius: within $1\,R_e$ ($R < 16\overset{''}{.}5$, panel a), between $1\,R_e$ and $2\,R_e$ (panel c), and within $2\,R_e$ (panel e). Panel g) presents the CMDs of a control field of similar area located at $\sim 7.5\,R_e$ from the center of NGC 1052-DF4. Right panels b), d), and f): LFs (all normalized to peak at one; black histograms) and filter responses (colored lines). These were used to identify the location of the TRGB, which is marked by the horizontal lines in the left panels. Panel h) presents the superposition of the three LFs (using the same color used to display the corresponding filter curve) compared to the control field (in red). While the jump in the LF due to TRGB clearly happens at very similar magnitude for the first three curves, the control field presents a significantly different distribution, with the LF peaking ≈ 1 mag fainter.

4. Distances to the Brightest Galaxies in the FOV of NGC 1052

Unfortunately, none of the brightest galaxies in the FOV of NGC 1052 (i.e., $R < 30$ arcmin centered on this object) has the distance estimated using the TRGB method. This implies that their distances have been measured using less reliable techniques, such as the SBF or the Tully–Fisher relation.

4.0.1. The Distance to NGC 1042

The distance to NGC 1042 has been measured using different methods. On one hand, there have been attempts to measure the distance using the reconstruction of the large-scale structure along the line of sight of the object. The most accurate measurement, which made a full model of the peculiar velocity to the Galaxy within 80 Mpc and also corrects the peculiar velocity of NGC 1042, provides a distance of 13.2 Mpc (parameter d_k^c in Table 5 of Theureau et al. 2007). On the other
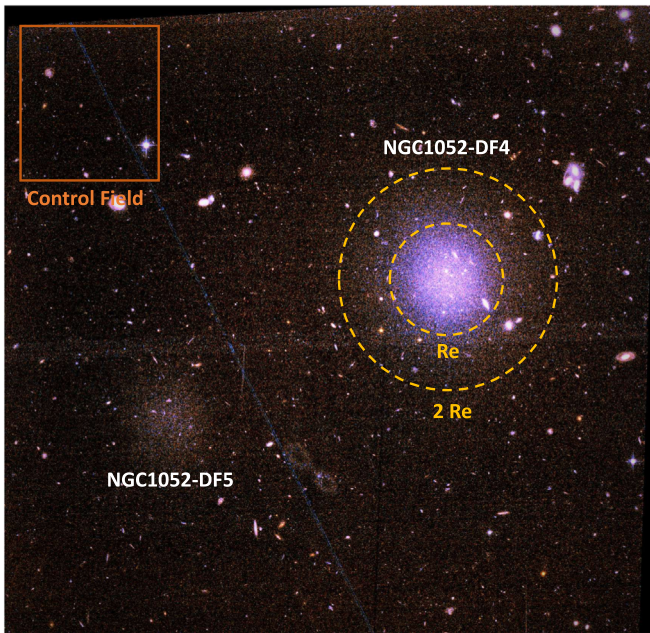
Figure 2. Color composite image of the ACS data used in this work showing the location of the galaxies NGC 1052-DF4 and NGC 1052-DF5. The regions enclosing 1 and 2 R_e of DF4 are shown using dashed yellow circles. The location on the control field is indicated with an orange square.

hand, the distance to the galaxy has been explored by mean of the Tully–Fisher relation. This last approach is the one producing a larger scatter on the values to the system, ranging from ∼4 (Tully et al. 2008) to ∼8 (Tully et al. 1992) Mpc. The main reason for this uncertainty is the lack of an accurate estimation of the inclination of the galaxy. In fact, values as low as 37° have been measured (Luo et al. 2016, based on Two Micron All Sky Survey photometry) but also larger values have been also provided (57°; Tully et al. 2008). The reason for such discrepancies is that the axis ratio and position angle of the galaxy change along the radial distance due to the presence of a bar and the spiral arms of the object (see Figure 4). To overcome this difficulty and have an accurate estimation of the inclination of NGC 1042, it is necessary to measure the ellipticity of the isophotes of the galaxy in its outer parts, a region where the internal structure of the galaxy is not playing any role.

In order to provide an accurate estimation of the Tully–Fisher distance to this object we have measured the inclination of the galaxy at its periphery ($155'' < R < 195''$). At such a radial distance the galaxy is not affected by the internal complex structure. In fact, both the axis ratio and the position angle remain pretty stable at such a location (see Figure 4). We have followed the recipe provided by Tully & Courtois (2012) to get the distance to the object. This recipe requires three parameters. The first is a) a measure of the rotation of the galaxy by using the 21 cm H I spectral line. For that, we use the value provided by van Gorkom et al. (1986) in their Figure 14 (i.e., $V_{max} - V_{min} \sim 145 \, (\sin i)^{-1} \, \mathrm{km \, s}^{-1}$). The second is b) the apparent luminosity of the galaxy given in the I-band; and finally, c) the inclination of the galaxy obtained from the ellipticity of the photometric image.

As a proxy for the I-band, we use the Sloan Digital Sky Survey (SDSS) i-band. We have retrieved the g-, r-, and i-band from the SDSS survey. This data is deep enough to provide accurate photometry down to 26.5 mag arcsec^{-2} (r-band;

Pohlen & Trujillo 2006). We use the axis ratio of the isophotes in the i-band to estimate the axis ratio of the galaxy. In particular, we use the average value of the axis ratio of the isophotes in the radial range $155'' < R < 195''$. The mean axis ratio is 0.832 ± 0.004. In Figure 4, we plot the shape of an elliptical contour with such an axis ratio at a radial distance of $190''$. The contour represents very well the outer part of the object. Once we have the axis ratio, we estimate the inclination of the galaxy using the following expression: $\cos i = [((b/a)^2 - q_0^2)/(1 - q_0^2)]^{1/2}$ with $q_0 = 0.2$ (Tully & Courtois 2012). This results in $\cos i = 0.824$ (i.e., $i = 34°.4$).

In order to measure the I-band magnitude of the galaxy, we apply the following transformation from the SDSS photometry to the Cousin system: $I = r - 1.2444 \times (r-i) - 0.3820$ (http://classic.sdss.org/dr5/algorithms/sdssUBVRITransform.html#vega_Sun_colors, see the entry "Lupton (2005)"). The SDSS apparent (AB) magnitudes that we measure correspond to the integrated magnitudes down to the i-band 26 mag arcsec^{-2} isophote. These are: 11.24 ± 0.05 mag (g-band), 10.80 ± 0.05 mag (r-band), and 10.48 ± 0.05 mag (i-band). This results in $I = 10.02 \pm 0.07$ mag. We can compare this value with the one provided for this galaxy in the Extragalactic Distance Database (EDD) catalog ($I = 10.19$ mag; column 23 in Table 1 of Tully et al. 2008). Using the following Galactic extinction correction for the SDSS filters (0.065 and 0.049 mag; r- and i-bands, respectively), the observed Vega I-band magnitude after correcting the Galactic extinction is 9.97 ± 0.07 mag. To correct for the effect of the internal extinction of NGC 1042 we use the following expression: $A_i' = \gamma_I \log(a/b)$, where a/b is the major to minor axis ratio and γ_I is given by Tully & Courtois (2012):

$$\gamma_I = 0.92 + 1.63(\log(V_{max} - V_{min}) - 2.5) \qquad (2)$$

obtaining $\gamma_I = 0.725$, so $A_i' = 0.068$ mag. The result of applying the internal and Galactic extinction correction is $I = 9.91$ mag for NGC 1042.

Finally, we measure the distance modulus to NGC 1042 using the following expression (Tully & Courtois 2012):

$$\mu = I - M_I = I + 21.39 + 8.81(\log(V_{max} - V_{min}) - 2.5) \qquad (3)$$

which results in $\mu = 30.24 \pm 0.41$ and a distance of 12.6 ± 2.3 Mpc. Using the I magnitude provided in the EDD catalog would give 13.5 ± 2.6 Mpc. In order to have the galaxy located at 19 Mpc, the inclination of the object would need to be as low as 26.7 deg (b/a = 0.898),[8] which is incompatible with the shape of its external isophotes (see Figure 4). Moreover, at all radial distances the inclination of the galaxies is not compatible with being close to a face-on projection as suggested by van Dokkum et al. (2019b). Finally, it is worth noting that the Tully–Fisher distance of NGC 1042 is compatible, within the error bars, with the distance obtained from the large-scale structure reconstruction (13.2 Mpc; Theureau et al. 2007).

4.0.2. The Distance to NGC 1052 and NGC 1047

The distance to NGC 1052 has been estimated using the SBF technique both in the I-band (19.4 ± 2 Mpc; Tonry et al. 2001)

---

[8] Using the EDD I-band magnitude, $I = 10.19$ mag, the inclination would need to be 28°.0 (b/a = 0.888), which again is far away from the observations.
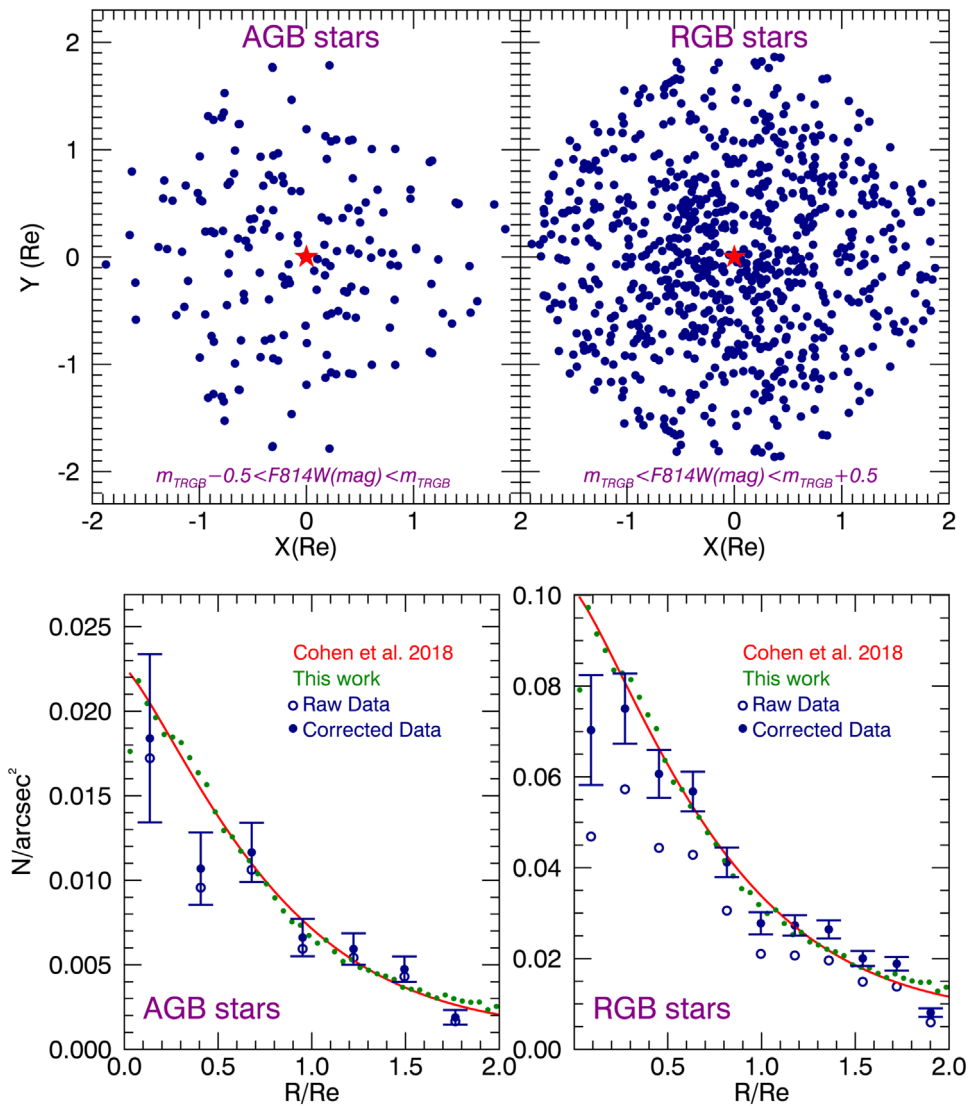
Figure 3. Spatial distribution and radial profiles of the stars detected above (AGBs) and below (RGBs) the TRGB of NGC 1052-DF4. Top panels: spatial distribution around the central position of the galaxy (red cross). The distance is indicated in R_e units. Note how the stars found tend to group around the central part of NGC 1052-DF4 as expected. Bottom panels: number density profiles of the stars detected around the TRGB. Open blue symbols correspond to the number density of the stars detected without applying any completeness correction, while solid blue symbols are the number of stars estimated after the completeness correction. Overplotted to the radial profiles of the stars is the surface brightness profile of the galaxy obtained using the `IRAF ELLIPSE` code (green points) and the Sérsic model fit to the surface brightness distribution provided in Cohen et al. (2018; red line).

and in the *F160W*-band (18 ± 2 Mpc; Jensen et al. 2003). The two results agree on a distance compatible with ∼19 Mpc.[9] Interestingly, NGC 1052 is interacting with another galaxy in the FOV: NGC 1047. This is clearly shown in the Dragonfly deep image of the group shown in Figure 4 of van Dokkum et al. (2019a) and the deep image by the Heron telescope provided in Figure 1 of Müller et al. (2019). This interaction is also very likely responsible for the perturbed distribution of H I around NGC 1052 found in van Gorkom et al. (1986). In fact, this idea fits very well with the tail of H I gas of NGC 1052 directly pointing to NGC 1047 (see Figure 5 of van Gorkom et al. 1986). It is worth noting that the distance quoted in the literature for NGC 1047 of 4.6 Mpc (Bottinelli et al. 1984) is clearly incompatible with the ongoing interaction between this object and NGC 1052.

4.0.3. The Distance to NGC 1035

Another bright galaxy in the FOV of NGC 1052 is the spiral NGC 1035. This galaxy is particularly interesting due to its vicinity to NGC 1052-DF4. The most recent Tully–Fisher distance determination for this galaxy has been obtained by Sorce et al. (2014). These authors quote a selection-bias-corrected distance estimate of 14 ± 2.9 Mpc for NGC 1035. This makes the galaxy distance compatible with NGC 1042.

Finally, there is another bright galaxy located at 28′.1 from NGC 1052: NGC1069. This object, however, has a heliocentric radial velocity of ∼9400 km s^{-1}, which makes it incompatible with being physically associated either to NGC 1042 or NGC 1052. The distance estimations for the galaxies in the FOV of NGC 1052 are summarized in Table 1 and Figure 5.
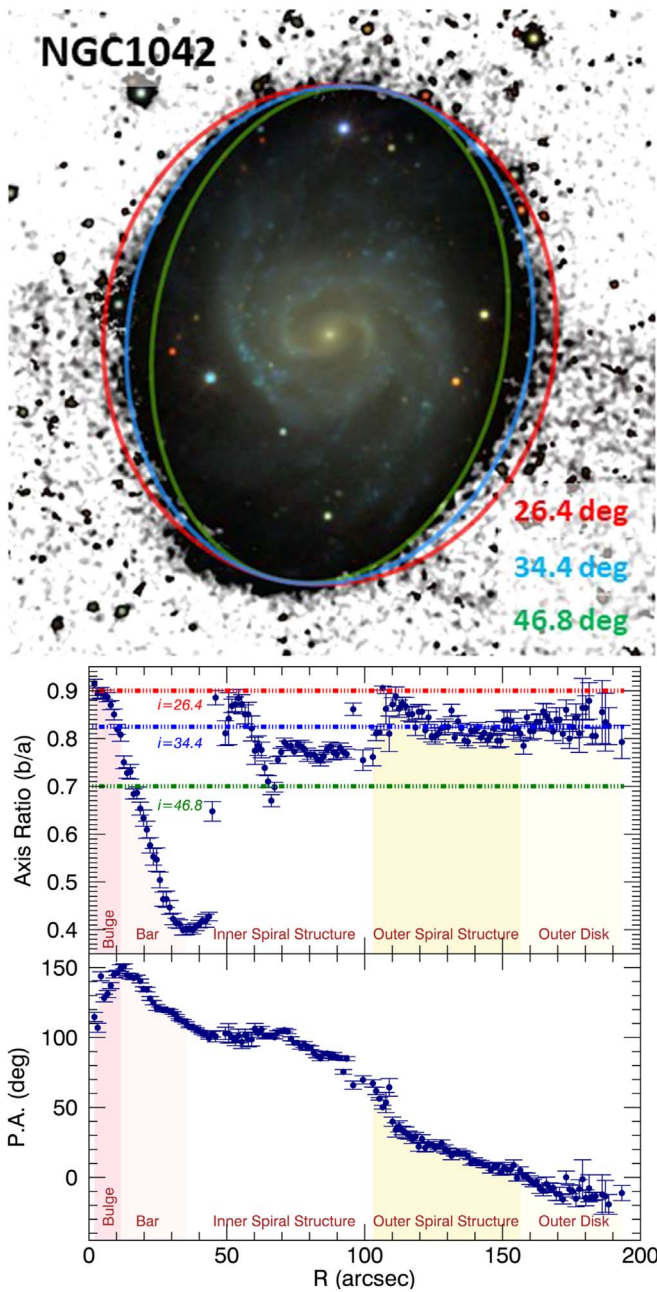
---

9 The large-scale structure reconstruction done by Theureau et al. (2007) also gives a compatible distance of 17.4 Mpc for this object.

Figure 4. Inclination of NGC 1042. Having an accurate estimation of the inclination of NGC 1042 is key to attaining a reliable measurement of the distance to the galaxy through the Tully–Fisher relation. The top panel shows the Sloan Digital Sky Survey (SDSS) image of NGC 1042 with three elliptical contours overplotted with different axis ratio. The image is a color composite of the SDSS filters g, r, and i, being the black and white background the sum of all the filters. The blue line corresponds to the inclination $34°.4$ that we measure in this work. Together with such an axis ratio, we show the corresponding ellipse representing the expected isophotal shape for an inclination of $26°.4$ (b/a = 0.9; red line) and $46°.8$ (b/a = 0.7; green line). For all cases we have assumed $q_0 = 0.2$ (see the text for details). The lower panel shows the axis ratio and position angle profiles of NGC 1042 obtained with the `IRAF ELLIPSE` package. Inclinations lower than 30 degrees are not favored by the shape of the external isophotes of the galaxy. A distance of 19 Mpc would require b/a = 0.898 (i.e., $26°.7$), which is ruled out by the observations.

5. Discussion

The results shown in this work reinforce the idea that the galaxies in the line of sight of NGC 1052 are grouped into two structures. We argue that the closest structure is formed by

NGC 1042 and NGC 1035 and contains the dwarf galaxies [KKS2000 04] and NGC 1052-DF4. This group of galaxies is located at $\sim$13.5 Mpc. In projection, we then have a second group, whose principal galaxy is NGC 1052 and also contains NGC 1047. This group is located at $\sim$19 Mpc. Despite being placed at different distances, the two groups share similar heliocentric velocities. When these velocities are transformed to the CMB rest frame, and therefore a comparison with the Hubble Flow can be conducted, we find the following. The average velocity of the two most massive galaxies located at $\sim$13.5 Mpc (NGC 1042 and NGC 1035) is 1100 km s^{-1} (i.e., the velocity of this group deviates from the expected Hubble Flow at that distance by $\sim$+150 km s^{-1}), while the average velocity of the two massive galaxies located at 19 Mpc (NGC 1047 and NGC 1052) is 1233 km s^{-1} (i.e., the departure from the Hubble Flow is $\sim$−100 km s^{-1}). In both cases, the absolute deviation from the Hubble Flow is very similar and not very large. We refer the reader to Trujillo et al. (2019) for an in-depth analysis of the largest discrepant galaxy [KKS2000 04]. In short, the values of the velocities of the galaxies in these two groups are not at all unexpected considering the typical peculiar velocities, in comparison to the Hubble flow, observed among the nearby galaxies (see a discussion about this in Section 5 of Trujillo et al. 2019). A distance of 13.5 Mpc would also mean that the globular clusters of DF4 would have a less extreme nature. Their intrinsic brightness would be fainter and their sizes would be smaller, going from a median size of 4.1 pc (van Dokkum et al. 2019a) to 2.8 pc, which is in better agreement with the median size of both globular clusters in the Milky Way ($2.9^{+0.1}_{-0.2}$ pc) and dwarf galaxies ($3.2^{+0.1}_{-0.2}$ pc; see, e.g., Trujillo et al. 2019).

Finally, it is worth mentioning how the effect of the distance impact on the claim of the dark matter content of NGC 1052-DF4. van Dokkum et al. (2019a) inferred a distance for this galaxy of 20 Mpc (see also a discussion in Haghi et al. 2019). With the TRGB distance measured here, 14.2 ± 0.7 Mpc, the dynamical mass of the galaxy (assuming an isothermal dark matter halo) decreases by a factor of 20/14.2 (i.e., $\sim$1.4), while its stellar mass decreases by a larger factor of $10^{0.4 \times (31.505 - 30.761)}$ (i.e., $\sim$2). van Dokkum et al. (2019a) also assumed a $(M/L)_{\text{stars},V} = 2.0 \pm 0.5 \Upsilon_{\odot}$, while for these types of diffuse galaxies we find, based on their spectral energy distribution (from ultraviolet to infrared) and assuming a Chabrier initial mass function, a value of $(M/L)_{\text{stars},V} = 1.07^{+0.80}_{-0.54} \Upsilon_{\odot}$ (Trujillo et al. 2019), which decreases by another factor of two the stellar mass content.[10] The combination of these two factors would reduce the total stellar mass of NGC 1052-DF4 by a factor of $\sim$3, alleviating significantly the absence of dark matter previously reported. To end this discussion, it is also worth mentioning the strong relevance that the assumption on the shape of the dark matter halo has for measuring the dark matter content of these galaxies. In Trujillo et al. (2019), we showed that the total dark matter halo that can accommodate the dynamics of KKS2000 04 changes by a factor of $\sim$3 from $10^{9.1} M_{\odot}$ (using an NFW halo) to $10^{9.6} M_{\odot}$ (using a Burkert cored halo with core radius of 4 kpc). In short, the larger the core of the dark matter halo, the larger the amount of dark matter compatible with the observed dynamics. There is

---

[10] Ruiz-Lara et al. (2019) have recently measured spectroscopically the age and metallicity of [KKS2000 04]: 8.7 Gyr and [M/H] = −1.18. With these estimations and assuming a Chabrier initial mass function, $(M/L)_{\text{stars},V} = 1.56$ $\Upsilon_{\odot}$.

Table 1
Distances to the Galaxies in the FOV of NGC 1052

Name	R.A. (J2000)	Decl. (J2000)	Distance (Mpc)	A_{F606W} (mag)	A_{F814W} (mag)	v_{hel} (km s^{-1})	v_{CMB} (km s^{-1})	Method
			Diffuse Galaxies					
[KKS2000]04	02:41:46.8	−08:24:09.3	13.0 ± 0.4	0.060	0.037	1793 ± 2	1576 ± 2	TRGB
NGC 1052-DF4	02:39:15.1	−08:06:58.6	14.2 ± 0.7	0.062	0.038	1445 ± 4	1228 ± 4	TRGB
			Bright Galaxies					
NGC 1035	02:39:29.1	−08:07:58.6	14 ± 3	0.062	0.038	1262 ± 16	1045 ± 16	Tully–Fisher
NGC 1042	02:40:24.0	−08:26:01.0	12.6 ± 2.3	0.071	0.044	1371 ± 1	1155 ± 1	Tully–Fisher
NGC 1047	02:40:32.8	−08:08:51.4	19 ± 2	0.063	0.039	1415 ± 15	1198 ± 15	Physical association with NGC 1052
NGC 1052	02:41:04.8	−08:15:20.8	19 ± 2	0.066	0.041	1484 ± 6	1268 ± 6	SBF

Note. The foreground extinction in the *HST* bands *F606W* and *F814W* are indicated for reference. The velocity v_{hel} corresponds to the mean heliocentric radial velocity. In order to make a sensible comparison of the velocities of these galaxies with the Hubble Flow, we include also the velocities with respect to the cosmic microwave background (CMB) v_{CMB}, which have been estimated subtracting 217 km s^{-1} to v_{hel} taking into account the location on the sky of these galaxies and the solar motion of 370.06 km s^{-1} toward the direction defined by galactic coordinates (263°914, +48°2646). See HYPERLEDA (Makarov et al. 2014) for further details.
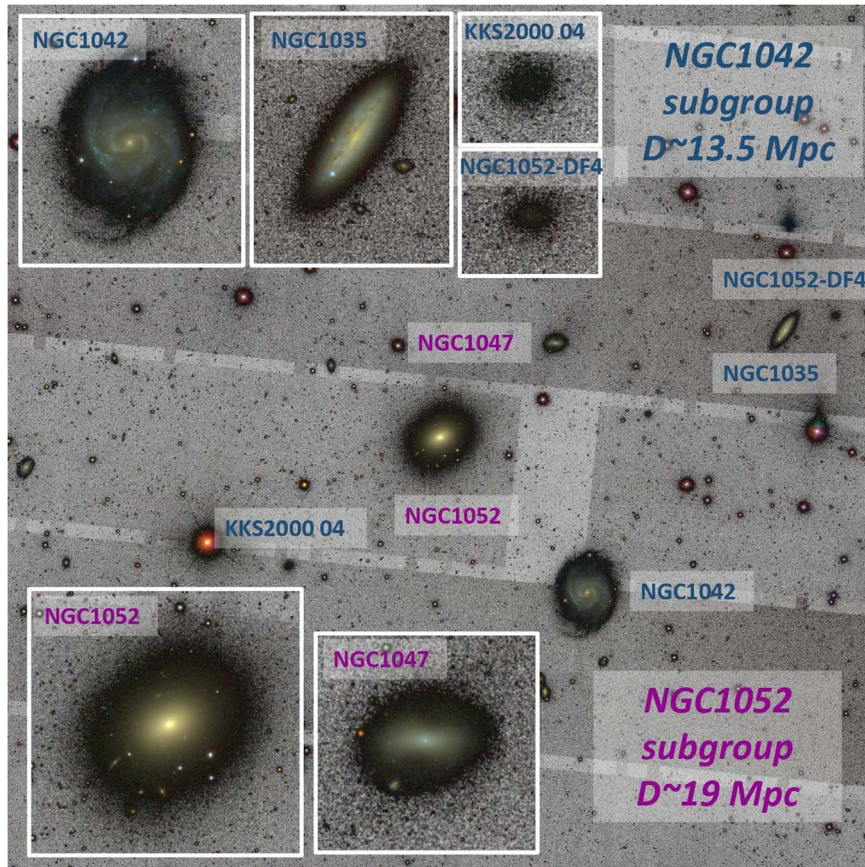

Figure 5. Distribution of the distances of the galaxies in the FOV of NGC 1052. The galaxies are distributed around two different distances, one at 13.5 Mpc containing NGC 1042 and NGC 1035 (and the dwarfs [KKS 2000] 04 and NGC 1052-DF4), and another group at 19 Mpc containing NGC 1052 and NGC 1047. The image is a color composite of the SDSS filters *g*, *r*, and *i*, being the black and white background the sum of all the filters.

growing evidence (both theoretical and observational) that the shape of the dark matter halo of the ultra-diffuse galaxies is probably dominated by an extended dark matter core (see for instance the works by Di Cintio et al. 2014; van Dokkum et al. 2019c). All in all, the proposition that both KKS2000 04 and NGC 1052-DF4 galaxies are "missing dark matter" is still far from having sure footing.

ORCID iDs

Matteo Monelli ⬤ https://orcid.org/0000-0001-5292-6380
Ignacio Trujillo ⬤ https://orcid.org/0000-0001-8647-2874

References

Aloisi, A., Clementini, G., Tosi, M., et al. 2007, ApJL, 667, L151
Blakeslee, J. P., & Cantiello, M. 2018, RNAAS, 2, 146
Blakeslee, J. P., Cantiello, M., Mei, S., et al. 2010, ApJ, 724, 657
Bottinelli, L., Gouguenheim, L., Paturel, G., & de Vaucouleurs, G. 1984, A&AS, 56, 381
Cantiello, M., Blakeslee, J. P., Ferrarese, L., et al. 2018, ApJ, 856, 126
Carlsten, S., Beaton, R., Greco, J., & Greene, J. 2019, ApJ, 879, 13
Cohen, Y., van Dokkum, P., Danieli, S., et al. 2018, ApJ, 868, 96
Di Cintio, A., Brook, C. B., Dutton, A. A., et al. 2014, MNRAS, 441, 2986
Haghi, H., Kroupa, P., Banik, I., et al. 2019, MNRAS, 487, 2441
Jensen, J. B., Tonry, J. L., Barris, B. J., et al. 2003, ApJ, 583, 712
Lee, M. G., Freedman, W. L., & Madore, B. F. 1993, ApJ, 417, 553
Luo, R., Hao, L., Blanc, G. A., et al. 2016, ApJ, 823, 85
Makarov, D., Prugniel, P., Terekhova, N., Courtois, H., & Vauglin, I. 2014, A&A, 570, A13
McQuinn, K. B. W., Skillman, E. D., Dolphin, A. E., Berg, D., & Kennicutt, R. 2017, AJ, 154, 51
Monelli, M., Hidalgo, S. L., Stetson, P. B., et al. 2010, ApJ, 720, 1225
Müller, O., Rich, R. M., Román, J., et al. 2019, A&A, 624, L6
Pohlen, M., & Trujillo, I. 2006, A&A, 454, 759
Rizzi, L., Tully, R. B., Makarov, D., et al. 2007, ApJ, 661, 815
Ruiz-Lara, T., Trujillo, I., Beasley, M. A., et al. 2019, MNRAS, 486, 5670
Sakai, S., Madore, B. F., & Freedman, W. L. 1996, ApJ, 461, 713
Sakai, S., Madore, B. F., Freedman, W. L., et al. 1997, ApJ, 478, 49
Salaris, M., & Cassisi, S. 1997, MNRAS, 289, 406
Skillman, E. D., Monelli, M., Weisz, D. R., et al. 2017, ApJ, 837, 102
Sorce, J. G., Tully, R. B., Courtois, H. M., et al. 2014, MNRAS, 444, 527
Stetson, P. B. 1987, PASP, 99, 191
Stetson, P. B. 1994, PASP, 106, 250
Theureau, G., Hanski, M. O., Coudreau, N., Hallet, N., & Martin, J.-M. 2007, A&A, 465, 71
Tonry, J. L., Dressler, A., Blakeslee, J. P., et al. 2001, ApJ, 546, 681
Trujillo, I., Beasley, M. A., Borlaff, A., et al. 2019, MNRAS, 486, 1192
Tully, R. B., & Courtois, H. M. 2012, ApJ, 749, 78
Tully, R. B., Shaya, E. J., Karachentsev, I. D., et al. 2008, ApJ, 676, 184
Tully, R. B., Shaya, E. J., & Pierce, M. J. 1992, ApJS, 80, 479
Turri, P., McConnachie, A. W., Stetson, P. B., et al. 2017, AJ, 153, 199
van Dokkum, P., Danieli, S., Abraham, R., Conroy, C., & Romanowsky, A. J. 2019a, ApJL, 874, L5
van Dokkum, P., Danieli, S., Cohen, Y., et al. 2018, Natur, 555, 629
van Dokkum, P., Danieli, S., Romanowsky, A., Abraham, R., & Conroy, C. 2019b, RNAAS, 3, 29
van Dokkum, P., Wasserman, A., Danieli, S., et al. 2019c, arXiv:1904.04838
van Gorkom, J. H., Knapp, G. R., Raimond, E., Faber, S. M., & Gallagher, J. S. 1986, AJ, 91, 791